Supporting Information

Reversible π-System Switching of Thiophene-fused Thiahexaphyrins by Solvent and Oxidation/Reduction

Tomohiro Higashino,* Atsushi Kumagai, Shigeyoshi Sakaki, Hiroshi Imahori*

Department of Molecular Engineering, Graduate School of Engineering, Kyoto University, Nishikyo-ku, Kyoto 615-8510, Japan

Fukui Institute for Fundamental Chemistry, Kyoto University, Sakyo-ku, Kyoto 606-8103, Japan.

Institute for Integrated Cell-Material Sciences (WPI-iCeMS), Kyoto University, Sakyo-ku, Kyoto 606-8501, Japan

t-higa@scl.kyoto-u.ac.jp, imahori@scl.kyoto-u.ac.jp

Contents

1. Experimental Section

Instrumentation and Materials.

Commercially available solvents and reagents were used without further purification unless otherwise mentioned. Silica-gel column chromatography was performed with UltraPure Silica Gel (230-400 mesh, SiliCycle) unless otherwise noted. Thin-layer chromatography (TLC) was performed with Silica gel 60 F_{254} (Merck). UV/Vis/NIR absorption spectra were measured with a Perkin-Elmer Lambda 900 UV/vis/NIR spectrometer. Steady-state fluorescence spectra were obtained by a HORIBA Nanolog spectrometer. ^{1}H, and ^{19}F NMR spectra were recorded with a JEOL EX-400 spectrometer (operating at 395.88 MHz for ^{1}H and 372.50 MHz for ^{19}F) by using the residual solvent as the internal reference for ^{1}H ($CDCl_3$: δ = 7.26 ppm, acetone-d_6: δ =2.05 ppm, DMF-d_7: δ = 8.03 ppm, THF-d_8: 3.58 ppm) and hexafluorobenzene as the external reference for ^{19}F (δ = –162.9 ppm). High-resolution mass spectra (HRMS) were measured on a Thermo Fischer Scientific EXACTIVE Fourier-transform orbitrap mass spectrometer (APCI). Single-crystal X-ray diffraction analysis data for compound **5** and **6** were collected at –150 °C on a Rigaku Saturn70 CCD diffractometer with graphite monochromated Mo-Kα radiation (0.71069 Å). The structures were solved by direct method (SHELXS-2014). Redox potentials were measured by cyclic voltammetry and differential pulse voltammetry method on an ALS electrochemical analyzer model 660A.

Density Functional Theory (DFT) Calculations.

All calculations were carried out using the *Gaussian 09* program.[S1] All structures were fully optimized without any symmetry restriction. The optimization were performed using the density functional theory (DFT) method with restricted B3LYP (Becke's three-parameter hybrid exchange functionals and the Lee-Yang-Parr correlation functional) level,[S2,S3] employing a basis set 6-31G(d,p) for C, H, N, F, and S. The relative total energies and MO diagrams are obtained using the single point calculations on the optimized structures at B3LYP/6-311G(d,p) level. The absolute ^{1}H shielding values were obtained using the GIAO method at the B3LYP/6-311G(d,p) level. The ^{1}H chemical shifts were calculated relative to $CHCl_3$ (δ = 7.26 ppm, absolute shielding: 24.96 ppm). Excitation energies and oscillator strengths on the optimized structures were calculated using the TD-SCF method at the B3LYP/6-311G(d,p) level.

2. Synthesis

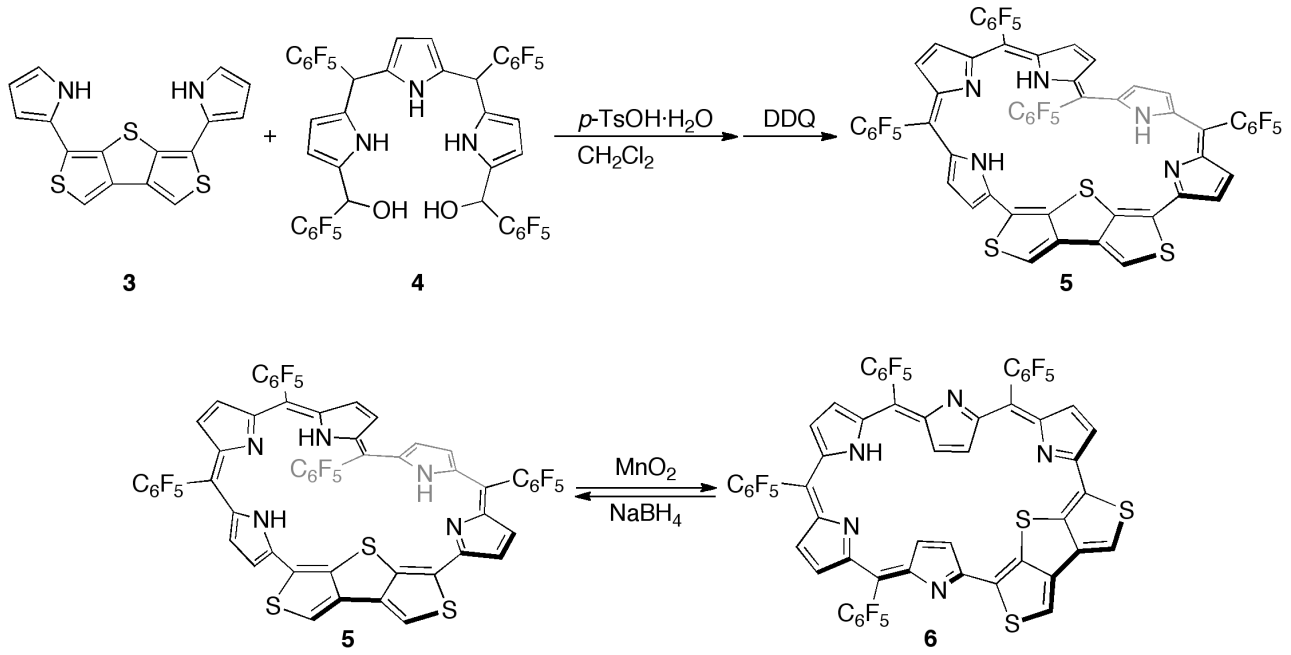

Scheme S1. Synthesis of thiophene-fused thiahexaphyrins.

3,5-Di(*N*-Boc-pyrrol-2-yl)dithieno[3,4-*b*:3′,4′-*d*]thiophene (**3**)[S4] and 1,14-bis(pentafluorobenzoyl)-5,10-bis(pentafluorophenyl)tripyrrane (**S1**)[S5] were prepared according to literature.

Thiophene-fused *meso*-(pentafluorophenyl)-31-thia[28]hexaphyrin (5):

1,14-Bis(pentafluorobenzoyl)-5,10-bis(pentafluorophenyl)tripyrrane (**S1**) (251 mg, 0.27 mmol) was reduced with $NaBH_4$ in a 10:1 mixture of THF and methanol. The reaction was quenched by addition of water, and the product was extracted with CH_2Cl_2. The combined organic layer was washed with water and brine, and dried over Na_2SO_4. The solvent was removed to yield dicarbiol (**4**) quantitatively, which was used instantly. *p*-Toluenesulfonic acid monohydrate (15.1 mg, 0.08 mmol) was added to a mixture of **3** (86.6 mg, 0.27 mmol) and **4** in dry CH_2Cl_2 (26.5 mL) and the reaction mixture was stirred for 3 h at room temperature under argon atmosphere. After adding 2,3-dichloro-5,6-dicyanobenzoquinone (DDQ, 120.3 mg, 0.54 mmol), the resulting mixture was stirred for 2 h. The reaction mixture was passed through an alumina column using CH_2Cl_2 as eluent. After the solvent was removed, the residue was separated by silica-gel column chromatography using a 1:2 mixture of CH_2Cl_2 and *n*-hexane to give **5** (22.4 mg, 18.2 μmol, 6.9%) as a wine red solid. Single crystals suitable for X-ray crystallographic analysis were obtained by vapor diffusion of *n*-hexane into a CH_2Cl_2 solution of **3**.

5: ^{1}H NMR (395.88 MHz, $CDCl_3$, 50 °C): δ = 13.09 (s, 1H, NH), 12.25 (s, 1H, NH), 9.97 (brs, 1H, NH),

7.67 (s, 1H, thienyl-H), 7.62 (s, 1H, thienyl-H), 6.94 (m, 2H, β-H), 6.81 (d, J = 4.2 Hz, 1H, β-H), 6.69 (d, J = 4.2 Hz, 1H, β-H), 6.52 (s, 1H, β-H), 6.48 (d, J = 4.2 Hz, 1H, β-H), 6.39 (d, J = 4.2 Hz, 2H, β-H), 6.31 (s, 1H, β-H), and 6.24 (s, 1H, β-H) ppm; (DMF-d_7, 25 °C): δ = 11.52 (brs, 1H, NH), 11.43 (s, 1H, NH), 10.27 (s, 1H, NH), 10.14 (s, 1H, β-H), 9.45 (s, 1H, β-H), 8.80 (s, 1H, β-H), 8.30 (s, 1H, β-H), 8.17 (s, 1H, thienyl-H), 7.93 (s, 1H, thienyl-H), 6.92 (d, J = 5.4 Hz, 2H, β-H), 6.74 (d, J = 4.2 Hz, 1H, β-H), 6.63 (d, J = 4.2 Hz, 1H, β-H), 6.49 (d, J = 4.2 Hz, 1H, β-H), and 6.34 (d, J = 4.2 Hz, 1H, β-H) ppm; ^{19}F NMR (372.50 MHz, $CDCl_3$, 25 °C): δ = –136.13 (br, 1F, *ortho*-F), –136.82 (br, 2F, *ortho*-F), –137.16 (br, 1F, *ortho*-F), –137.56 (br, 1F, *ortho*-F), –137.70 (d, J = 17.1 Hz, 2F, *ortho*-F), –139.74 (br, 1F, *ortho*-F), –151.57 (br, 1F, *para*-F), –151.88 (t, J = 17.1 Hz, 1F, *para*-F), –153.32 (br, 1F, *para*-F), –153.58 (t, J = 22.7 Hz, 1F, *para*-F), –159.66 (br, 2F, *meta*-F), –160.51 (m, 2F, *meta*-F), –160.73 (m, 2F, *meta*-F), –160.93 (m, 1F, *meta*-F), and –161.23 (m, 1F, *meta*-F) ppm. UV/vis (CH_2Cl_2): λ (ε, $M^{-1}\,cm^{-1}$) = 412 (34000), 539 (48000), and 734 (10000) nm; (acetone): λ (ε, $M^{-1}\,cm^{-1}$) = 385 (28000), 446 (38000), 537 (92000), 936 (11000), and 1032 (7400) nm; (DMF): λ (ε, $M^{-1}\,cm^{-1}$) = 380 (26000), 440 (32000), 556 (94000), 940 (14000), and 1044 (18000) nm. Fluorescence (CH_2Cl_2, λ_{ex} = 734 nm): λ_{max} = 955 nm. HRMS (APCI, positive) calcd. for $C_{56}H_{16}N_5F_{20}S_3$ $[M+H]^+$ 1234.0243; found 1234.0210.

Thiophene-fused *meso*-(pentafluorophenyl)-31-thia[26]hexaphyrin (6):

To a stirred solution of **5** (10.1 mg, 8.18 μmol) in CH_2Cl_2 (16 mL) was added MnO_2 (14.2 mg, 0.16 mmol) and the mixture was stirred for 1 h. The mixture was passed through a Celite pad and the solvent was removed. The crude product was purified by silica-gel column chromatography using CH_2Cl_2 to give **6** (10.0 mg, 8.12 μmol, 99%) as a dark red solid. Single crystals suitable for X-ray crystallographic analysis were obtained by vapor diffusion of *n*-nonane into a chlorobenzene solution of **6**.

6: ^{1}H NMR (395.88 MHz, $CDCl_3$, 25 °C): δ = 10.11 (br, 1H, NH), 7.95 (s, 1H, thienyl-H), 7.93 (s, 1H, thienyl-H), 7.73 (d, J = 4.8 Hz, 1H, β-H), 7.51 (d, J = 4.8 Hz, 1H, β-H), 7.27 (s, 2H, β-H), 6.96 (d, J = 4.8 Hz, 1H, β-H), 6.93 (d, J = 4.8 Hz, 1H, β-H), 6.90 (d, J = 4.8 Hz, 1H, β-H), and 6.67 (m, 3H, β-H) ppm; (THF-d_8, 25 °C): δ = 10.47 (br, 1H, NH), 8.39 (s, 1H, thienyl-H), 8.34 (s, 1H, thienyl-H), 7.93 (d, J = 4.8 Hz, 1H, β-H), 7.84 (d, J = 4.8 Hz, 1H, β-H), 7.50 (s, 2H, β-H), 7.12 (m, 2H, β-H), 7.06 (d, J = 4.8 Hz, 1H, β-H), 6.96 (d, J = 4.8 Hz, 1H, β-H), 6.94 (d, J = 4.8 Hz, 1H, β-H), and 6.90 (d, J = 4.8 Hz, 1H, β-H) ppm; ^{19}F NMR (372.50 MHz, $CDCl_3$, 25 °C): δ = –134.25 (d, J = 17.1 Hz, 2F, *ortho*-F), –136.79 (d, J = 22.7 Hz, 2F, *ortho*-F), –137.27 (d, J = 22.7 Hz, 2F, *ortho*-F), –137.61 (d, J = 17.1 Hz, 2F, *ortho*-F), –150.26 (t, J = 22.7 Hz, 1F, *para*-F), –152.32 (t, J = 17.1 Hz, 1F, *para*-F), –153.10 (t, J = 17.1 Hz, 1F, *para*-F), –153.78 (t, J = 22.7 Hz, 1F, *para*-F), –159,74 (m, 2F, *meta*-F), –161.26 (t, J = 22.7 Hz, 2F, *meta*-F),

–162.82 (t, J = 17.1 Hz, 2F, *meta*-F), and –163.13 (t, J = 22.7 Hz, 2F, *meta*-F) ppm. UV/vis (CH_2Cl_2): λ (ε, $M^{-1}\,cm^{-1}$) = 380 (32000), 487 (55000), 712 (11000) nm. Fluorescence (CH_2Cl_2, λ_{ex} = 712 nm): λ_{max} = 930 nm. HRMS (APCI, positive) calcd. for $C_{56}H_{14}N_5F_{20}S_3$ $[M+H]^+$ 1232.0086; found 1232.0083.

3. High-Resolution Mass Spectra

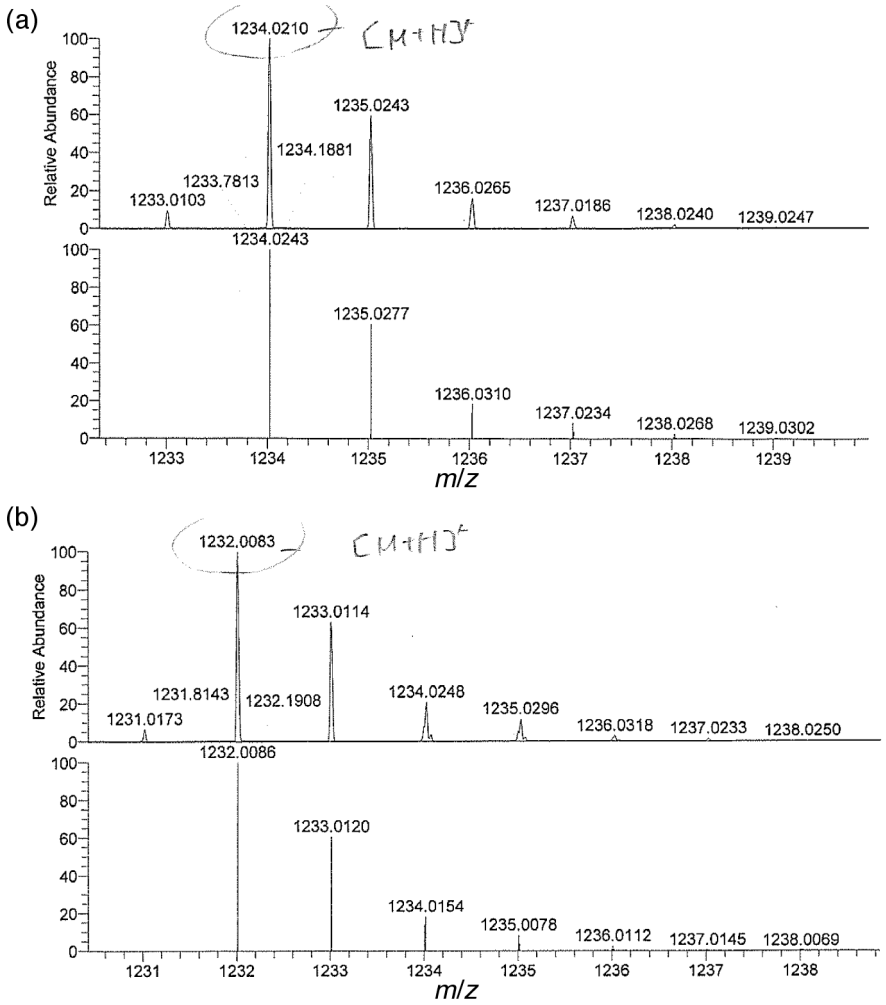

Figure S1. Observed (top) and simulated (bottom) high-resolution mass spectra of (a) **5** and (b) **6**.

4. NMR Spectra

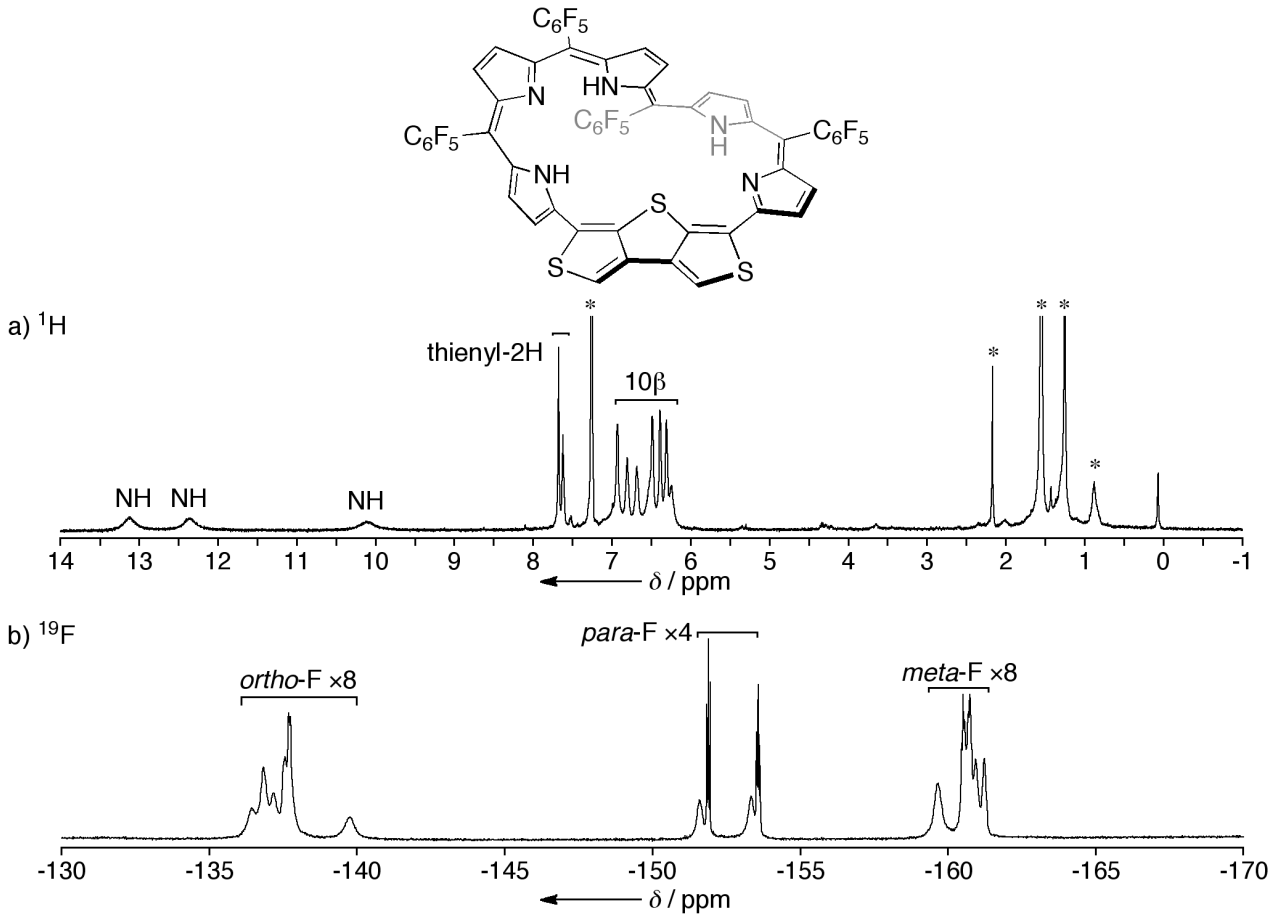

Figure S2. (a) ^{1}H and (b) ^{19}F NMR spectra of **5** at 25 °C in $CDCl_3$. Peaks marked with ∗ arise from residual solvents.

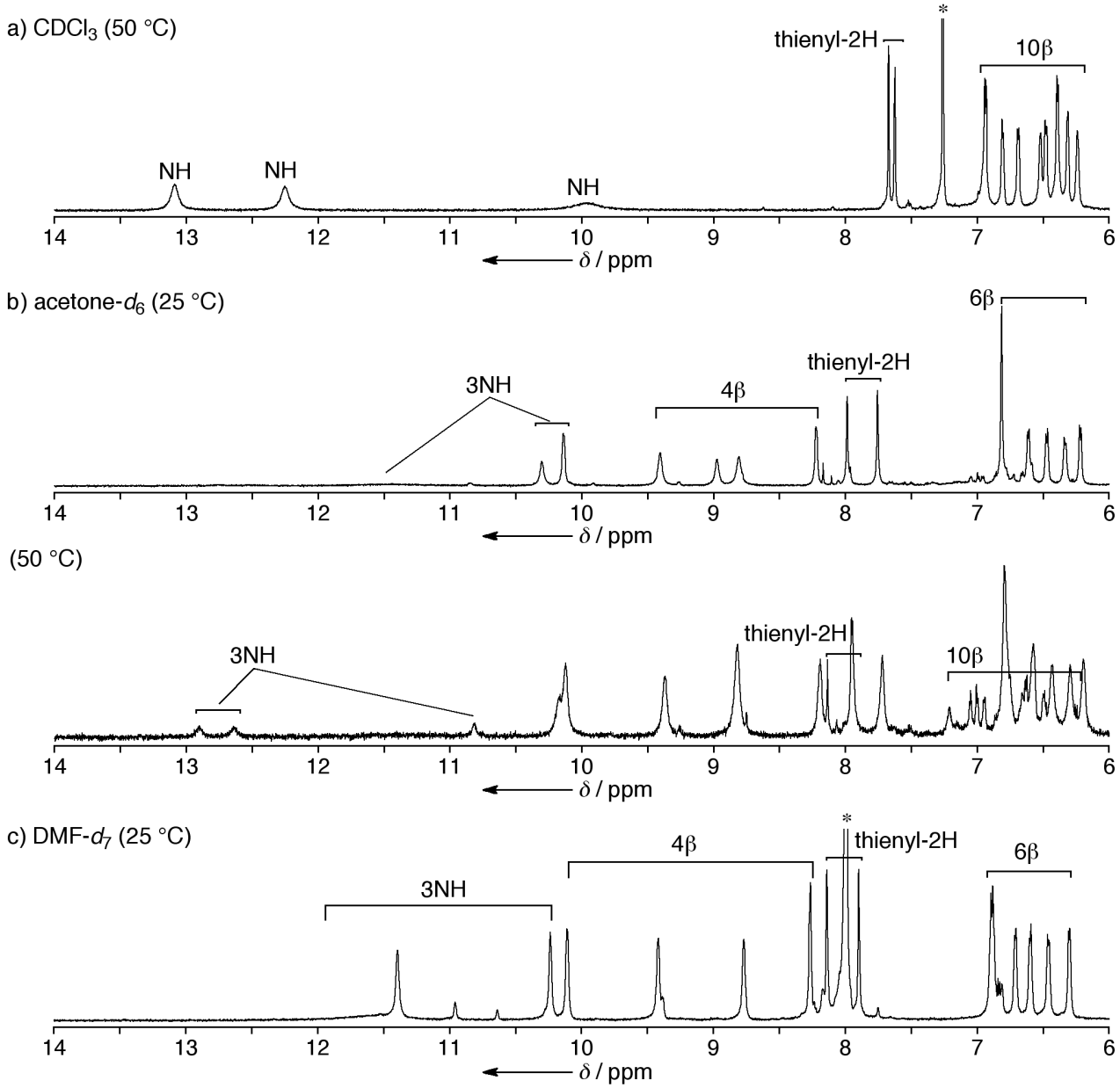

Figure S3. ^{1}H NMR spectra of **5** in (a) $CDCl_3$, (b) acetone-d_6, and (c) DMF-d_7. Peaks marked with ∗ arise from residual solvents. In acetone-d_6 at 50 °C, the signals derived from the nonaromatic species are shown. The minor peaks in DMF-d_7 suggest the existence of another conformation.

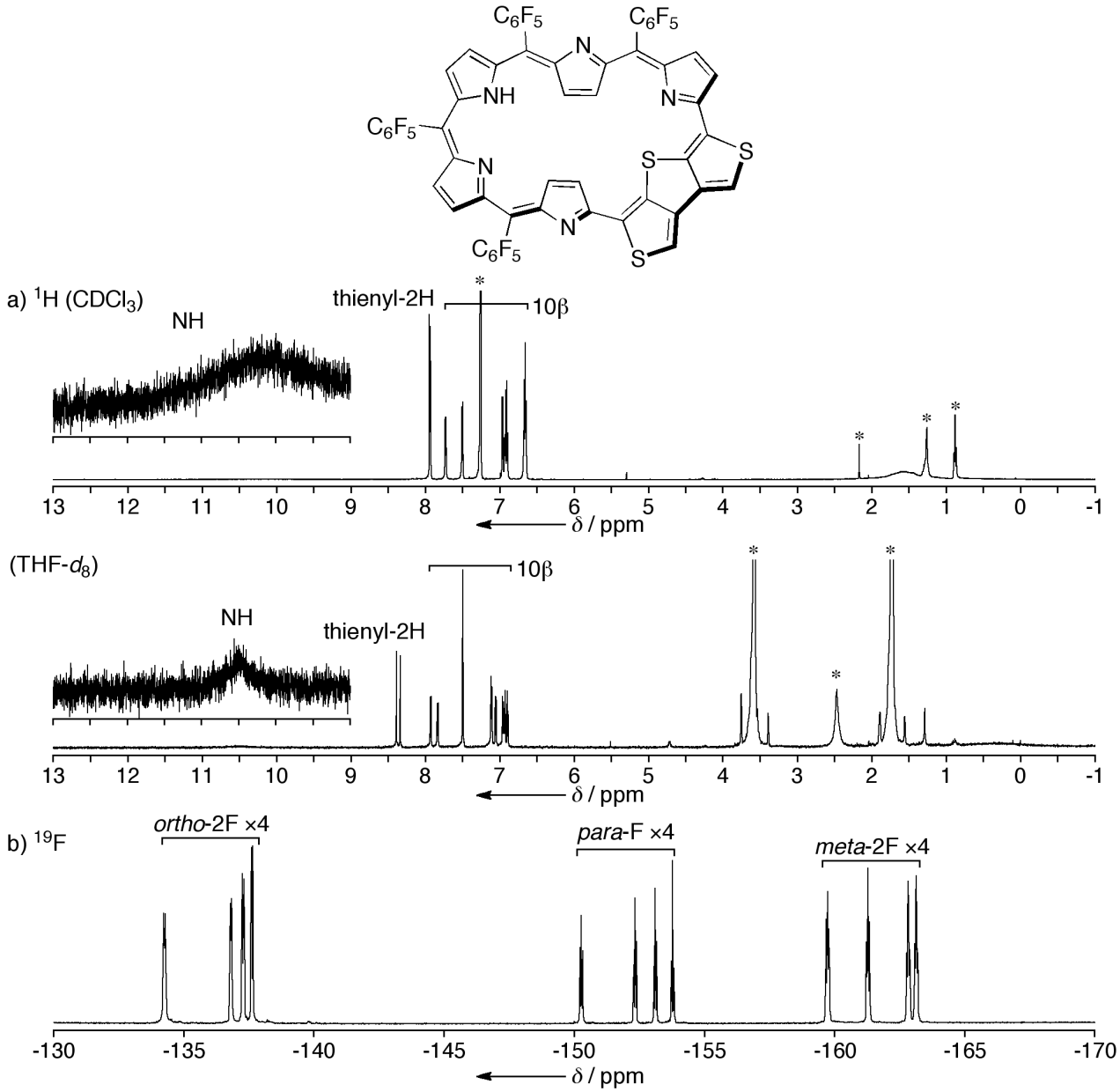

Figure S4. (a) ^{1}H NMR spectra in $CDCl_3$ and THF-d_8 and (b) ^{19}F NMR spectrum in $CDCl_3$ of **6** at 25 °C. Peaks marked with ∗ arise from residual solvents.

5. X-Ray Crystallographic Details

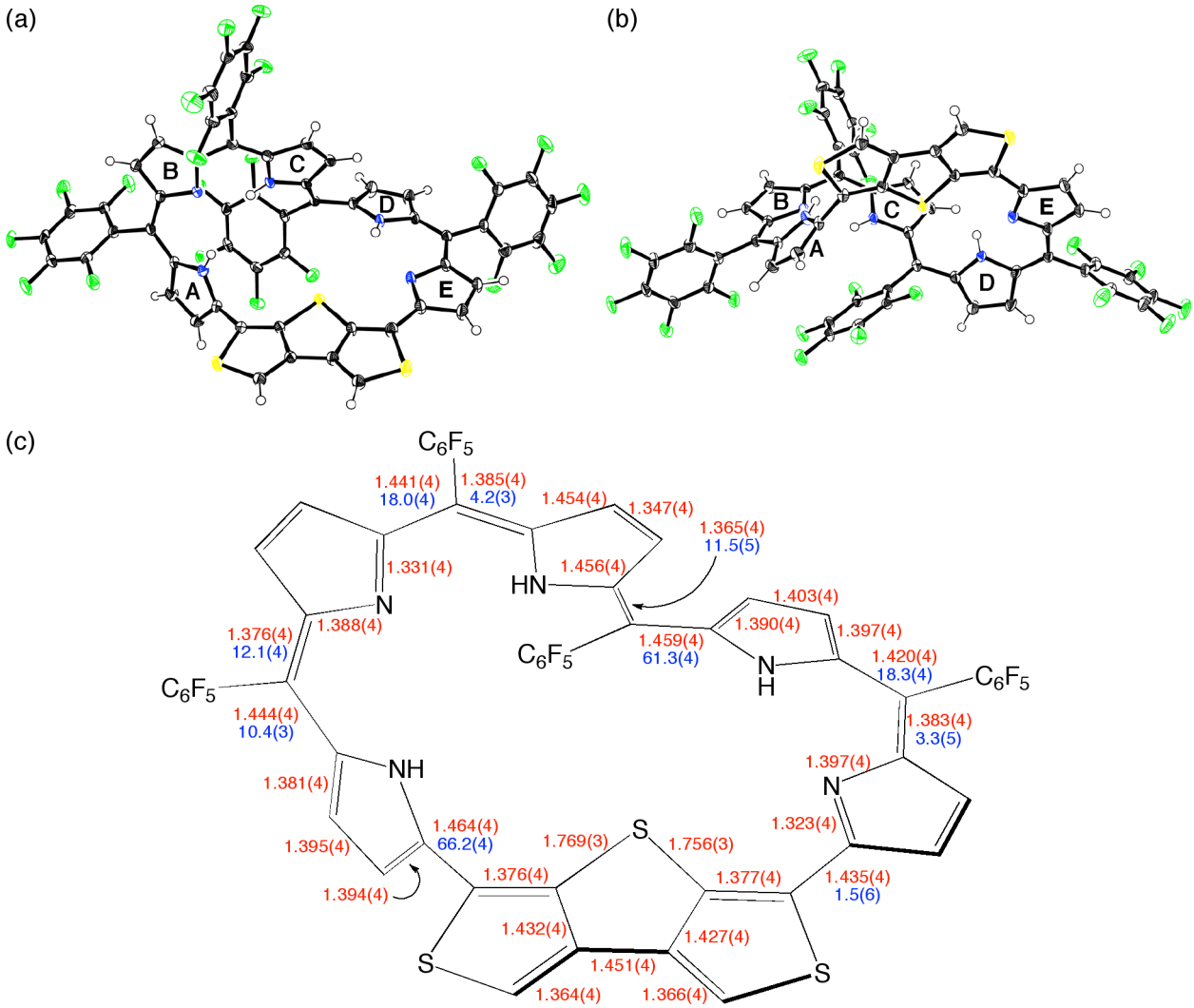

Figure S5. X-Ray crystal structure of **5**: (a) top view and (b) side view. Thermal ellipsoids represent 50% probability. Solvent molecules are omitted for clarity. (c) Detailed structural data of **5**. Selected bond lengths in Å (numbers in red) and torsion angles in degree (numbers in blue) are indicated.

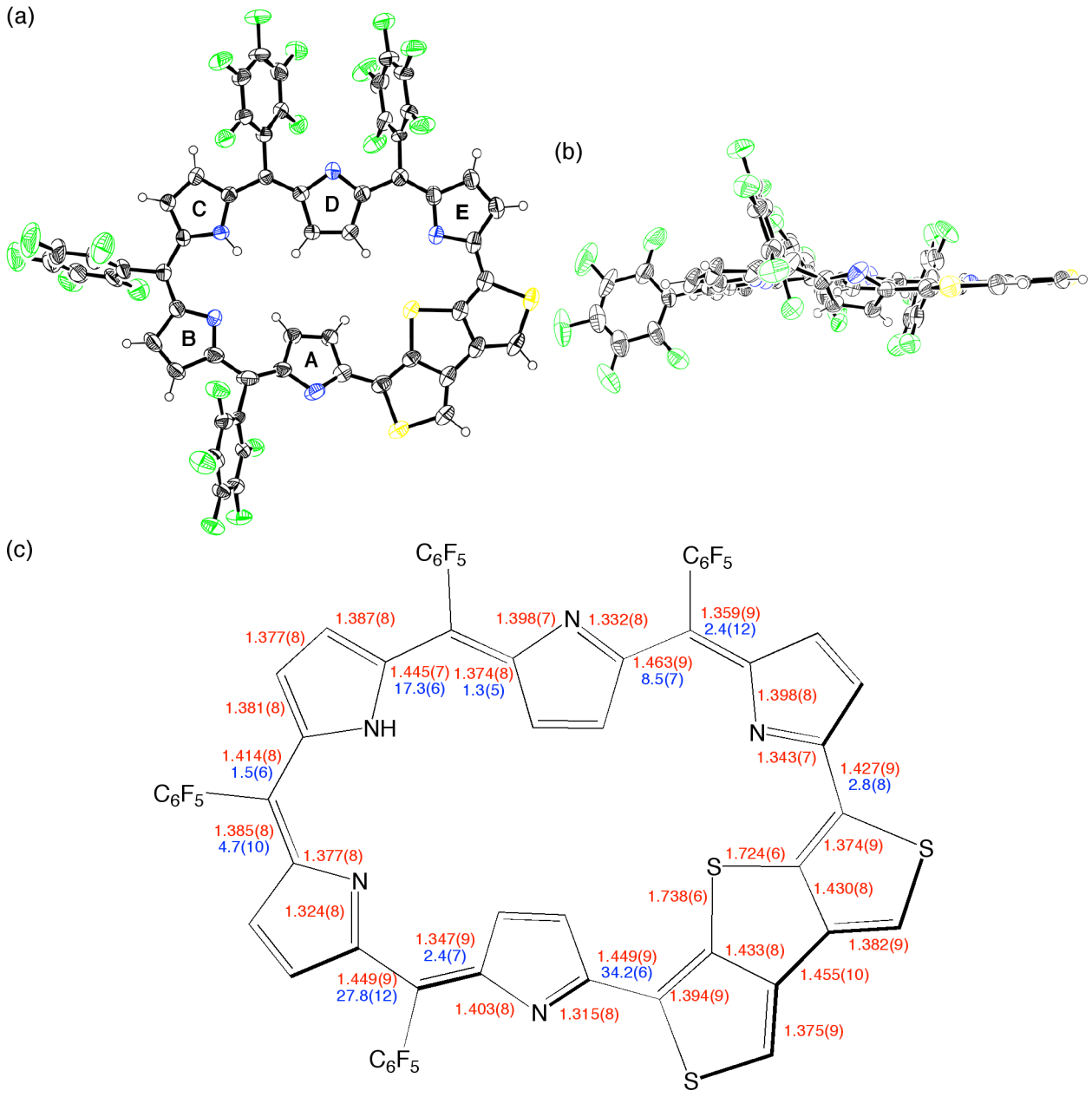

Figure S6. X-Ray crystal structure of **6**: (a) top view and (b) side view. Thermal ellipsoids represent 50% probability. One of the two independent molecules in the unsymmetric unit cell is shown. Minor disorder component and solvent molecules are omitted for clarity. (c) Detailed structural data of **6**. Selected bond lengths in Å (numbers in red) and torsion angles in degree (numbers in blue) are indicated.

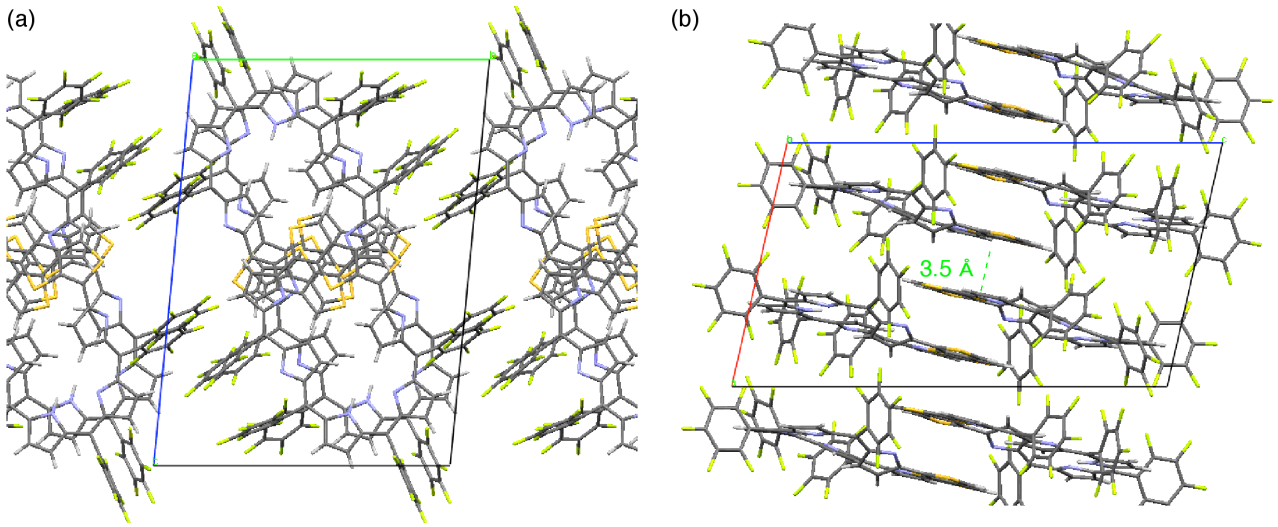

Figure S7. Packing structure of **6** along with (a) *a*-axis and (b) *b*-axis. Solvent molecules and minor disorder components are omitted for clarity.

Table S1. Crystal data of **5** and **6**.

	5	**6**
formula	$C_{56}H_{15}F_{20}N_5S_3$· 3.5(CH_2Cl_2)	2($C_{56}H_{13}F_{20}N_5S_3$)· 3(chlorobenzene)
M_r	1531.15	2796.40
T [K]	123(2)	123(2)
crystal system	triclinic	triclinic
space group	*P*-1 (No.2)	*P*-1 (No.2)
a [Å]	13.890(2)	13.765(3)
b [Å]	14.796(2)	17.271(3)
c [Å]	16.218(2)	24.190(5)
α [°]	96.6694(14)	94.738(3)
β [°]	96.2744(14)	102.606(4)
γ [°]	112.8223(16)	93.061(5)
V [Å^3]	3007.7(7)	5577.7(19)
Z	2	2
ρ_{calcd} [g cm^{-3}]	1.691	1.665
F [000]	1522	2786
crystal size [mm^3]	0.30×0.30×0.05	0.25×0.10×0.03
$2\theta_{max}$ [°]	54.98	54.00
reflections collected	24673	44377
independent reflections	13239	23504
parameters	921	1956
R_1 [$I > 2\sigma(I)$]	0.0621	0.1121
wR_2 [all data]	0.1921	0.3578
GOF	1.096	1.077
CCDC number	1841655	1841656

6. Optical Properties

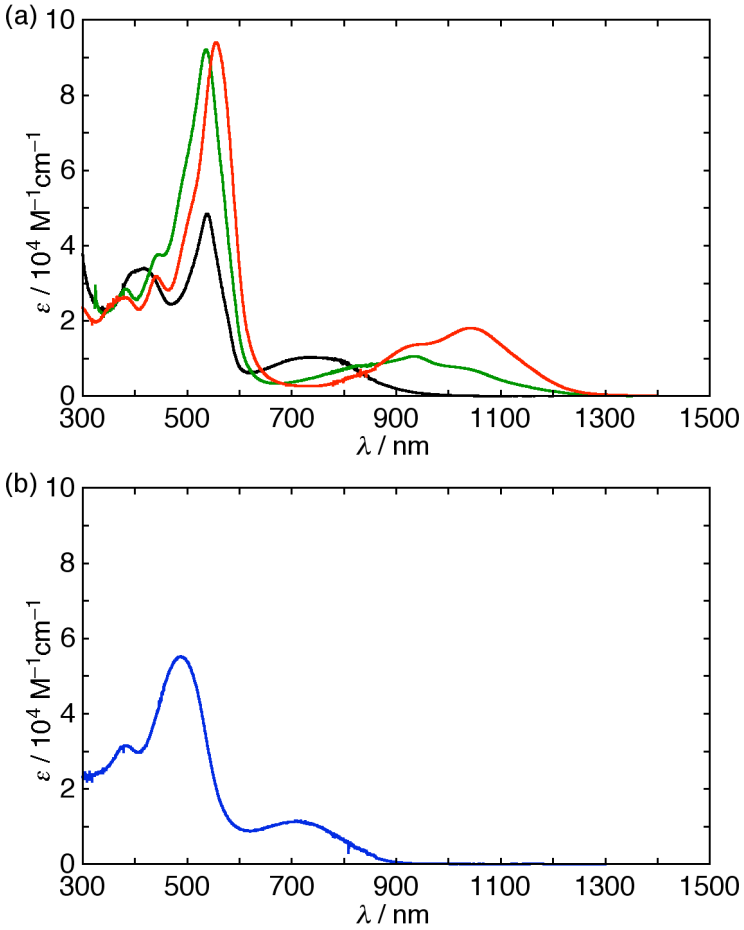

Figure S8. UV/Vis/NIR absorption spectra of (a) **5** in CH_2Cl_2 (black), acetone (green), DMF (red) and (b) **6** in CH_2Cl_2 (blue).

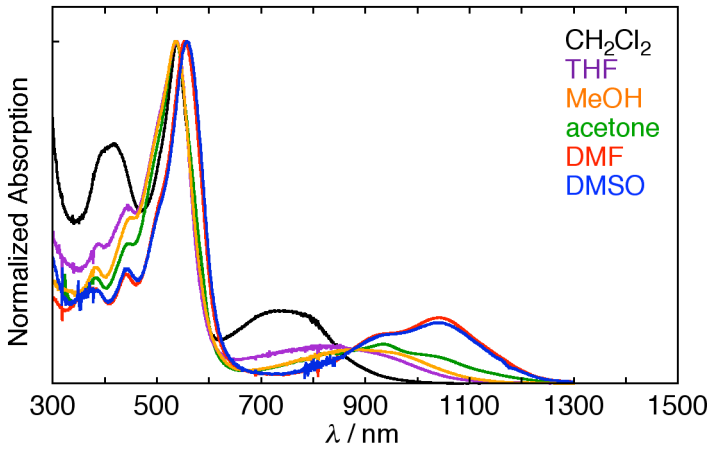

Figure S9. Normalized UV/vis/NIR absorption spectra of **5** in various solvents.

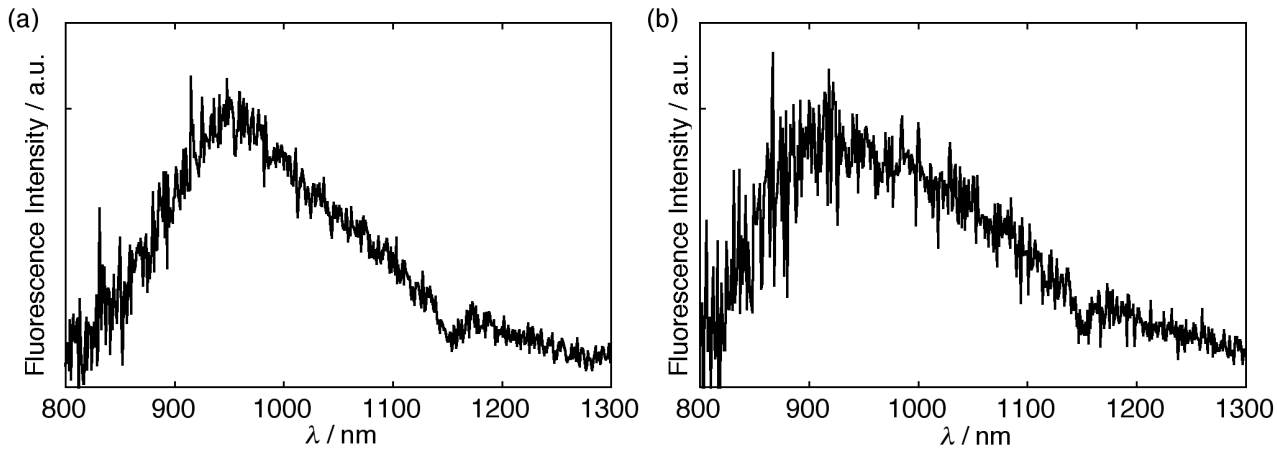

Figure S10. Fluorescence spectra of (a) **5** and (b) **6** in CH_2Cl_2. The samples were excited at the Q-like bands (734 nm for **5** and 712 nm for **6**).

7. Electrochemical Properties

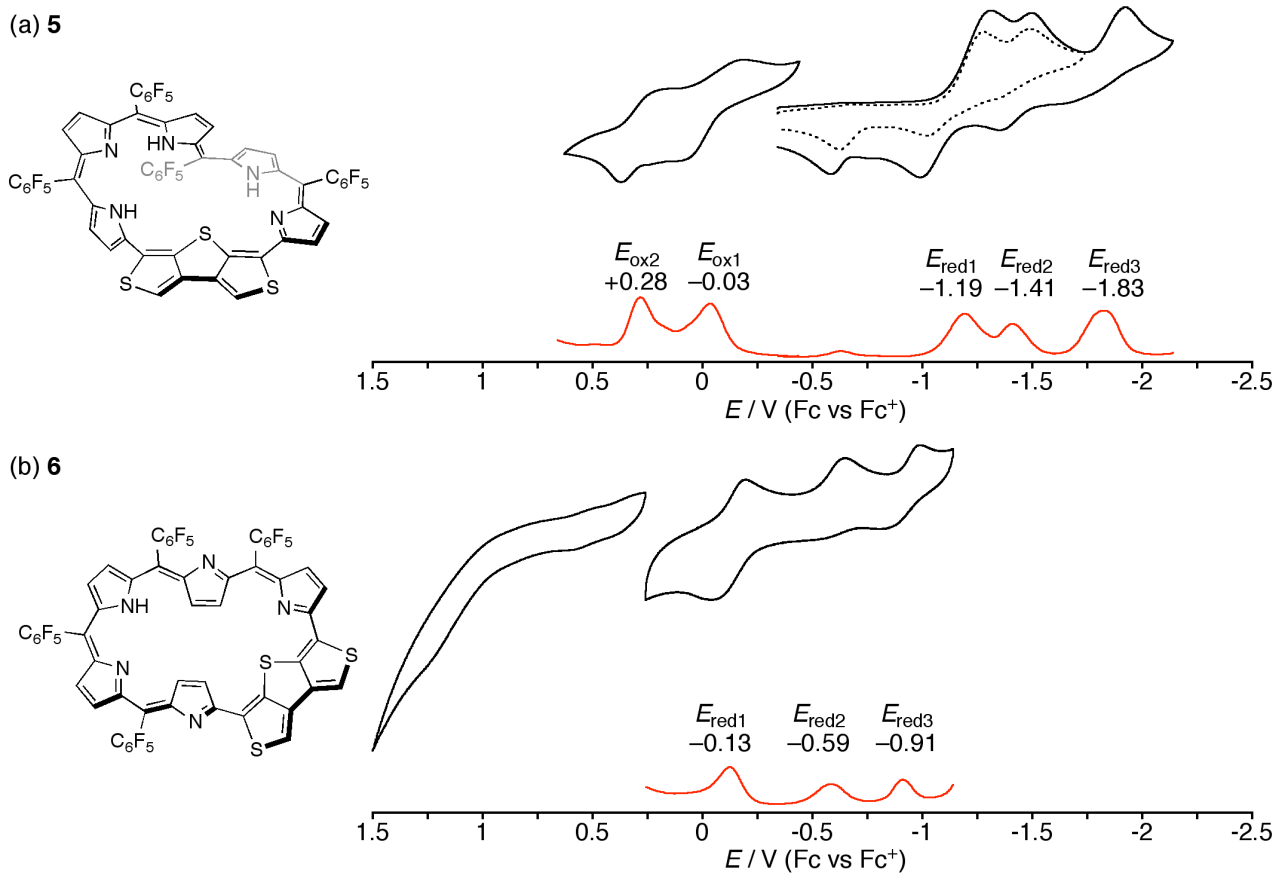

Figure S11. Cyclic voltammograms (black) and differential pulse voltammetry (DPV) curves (red) of hexaphyrins (a) **5** and (b) **6**. Redox potentials were determined by DPV. Solvent: CH_2Cl_2; scan rate: 0.05 V s^{-1}; working electrode: glassy carbon; reference electrode: Ag/Ag^+ (0.01 M $AgNO_3$); electrolyte: 0.1 M *n*-Bu_4NPF_6. Peaks marked with ∗ arise from oxygen.

8. DFT Calculations

Table S2. The relative total energies (kJ mol^{-1}) of **5a**-**d**.

	5a	**5b**	**5c**	**5d**
B3LYP/6-311G(d,p)	0	+18.4	+39.3	+39.5
CAM-B3LYP/6-311G(d,p)	0	+18.2	+44.6	+35.9
M06-2X/6-311G(d,p)	0	+14.2	+45.3	+37.5

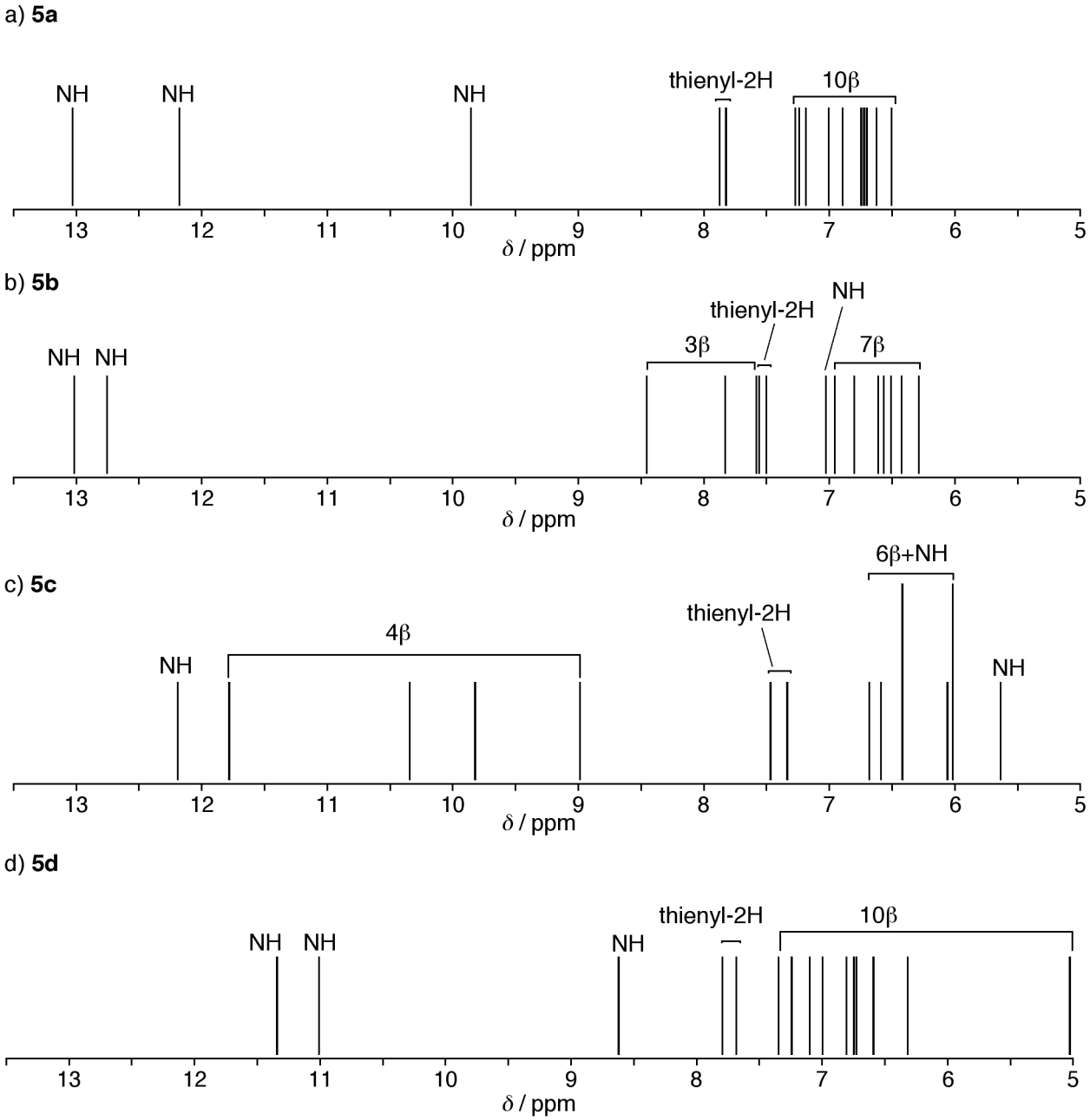

Figure S12. Simulated ^{1}H chemical shifts on optimized structures of (a) **5a**, (b) **5b**, (c) **5c**, and (d) **5d**. The calculations were carried out in gas phase because of weak solvation effect by $CHCl_3$. Indeed, the PCM model with $CHCl_3$ solvent shows little influences on the ^{1}H chemical shifts of **5a**.

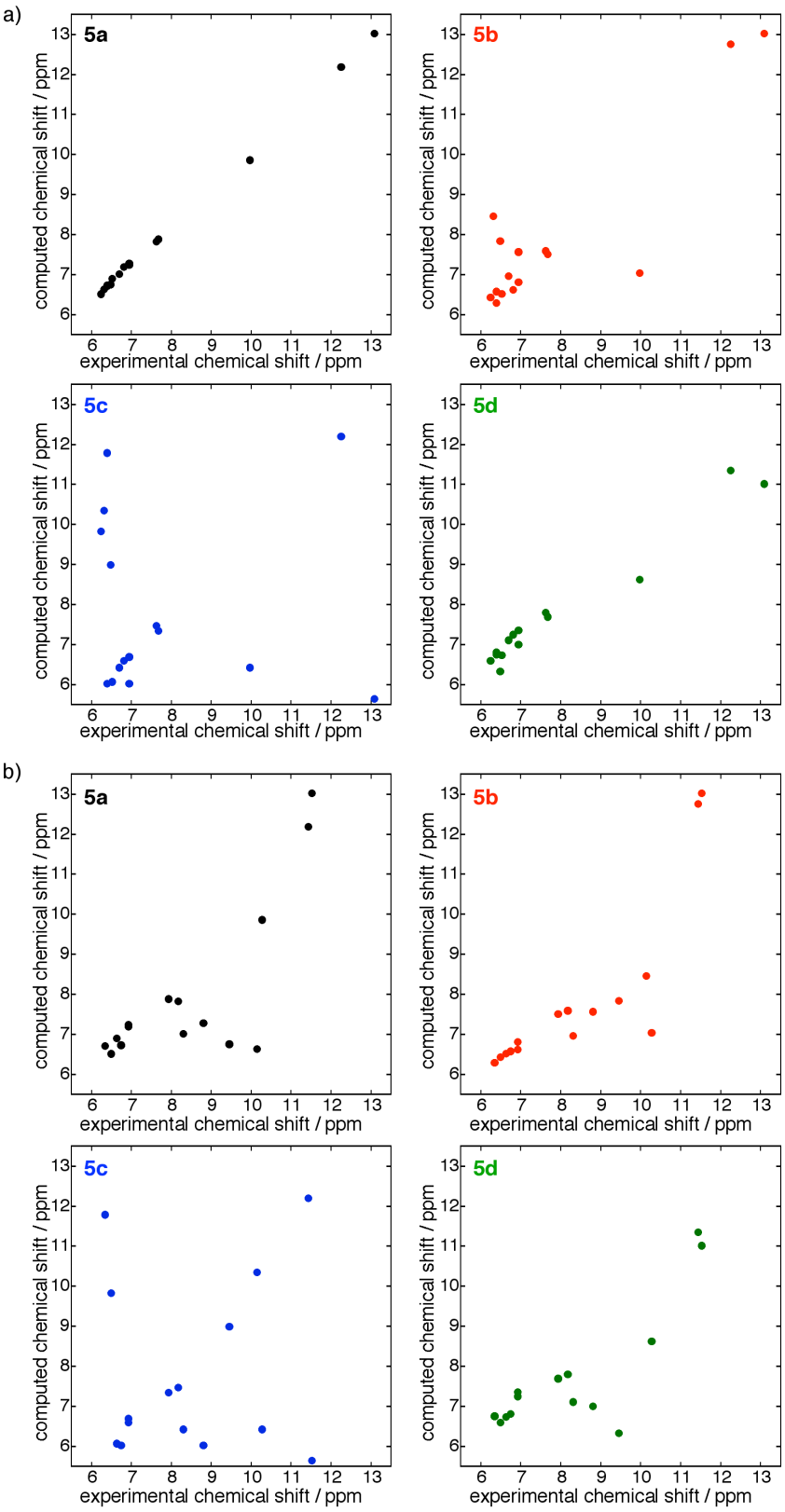

Figure S13. Plots of computed ^{1}H chemical shifts on optimized structures of **5a–d** versus experimental ^{1}H chemical shifts in (a) $CDCl_3$ and (b) DMF-d_7.

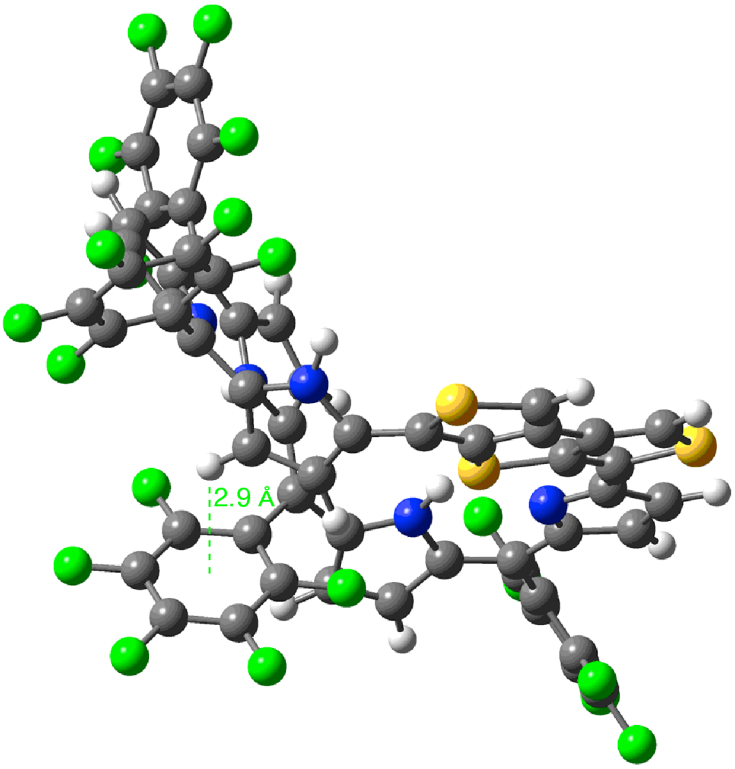

Figure S14. The optimized structure **5c**. The β-proton on pyrrole A is located over the pentafluorophenyl ring.

Table S3. The NICS values (ppm) at the gravity centers of the core 36 atoms (highlighted in red) on the optimized structures of hexaphyrins **5a-c** and **6** in gas phase or using PCM solvation model.

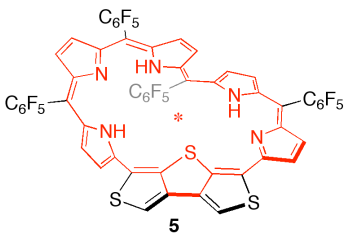

5

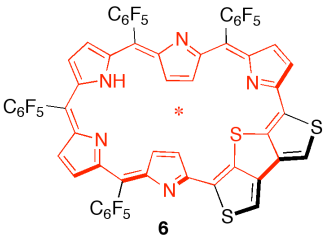

6

	5a	**5b**	**5c**	**5d**	**6**
gas phase	–0.57	–0.14	+2.48	–0.68	–2.52
PCM (CH_2Cl_2)	–0.56	–0.19	+2.33	–0.63	–2.44
PCM (DMSO)	–0.55	–0.21	+2.27	–0.62	–2.42

The computational studies reported that NICS values are more positive in solvents.[S6,S7] In fact, the NICS values of **5a**, **5d**, and **6** were shifted to positive direction in the solvents. However, the NICS values of **5b** and **5c** were shifted to negative direction. This opposite trend implies the unique π-electron system of **5b** and **5c**.

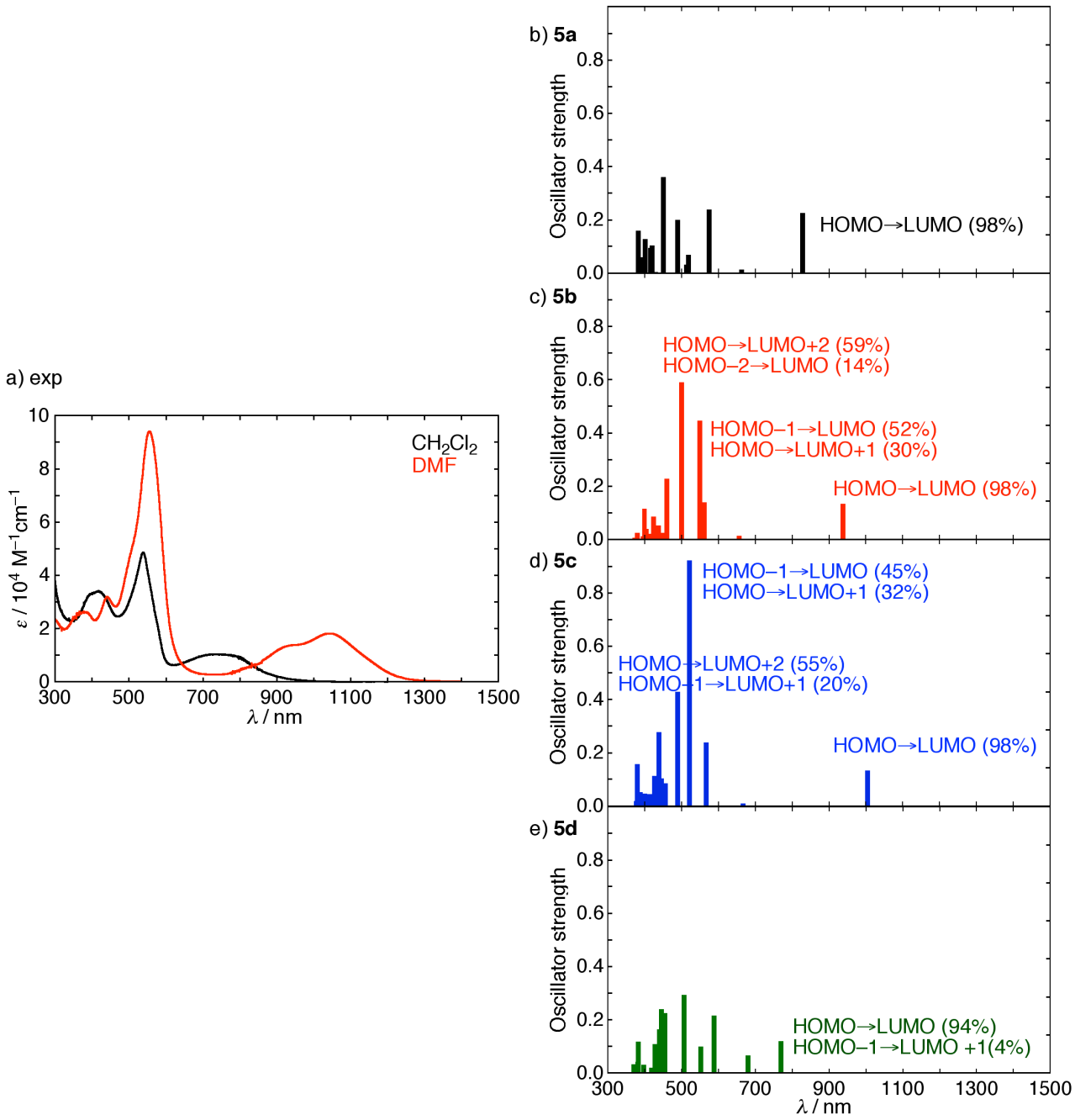

Figure S15. (a) The UV/vis/NIR absorption spectra of **5** in CH_2Cl_2 and DMF, and calculated excitation energies with oscillator strengths on conformations (b) **5a**, (c) **5b**, (d) **5c**, and (e) **5d**. The excitation weights of the lowest excitations are indicated. For **5b** and **5c**, excitation weights of the excitations with large oscillator strengths ($f > 0.4$) are also indicated.

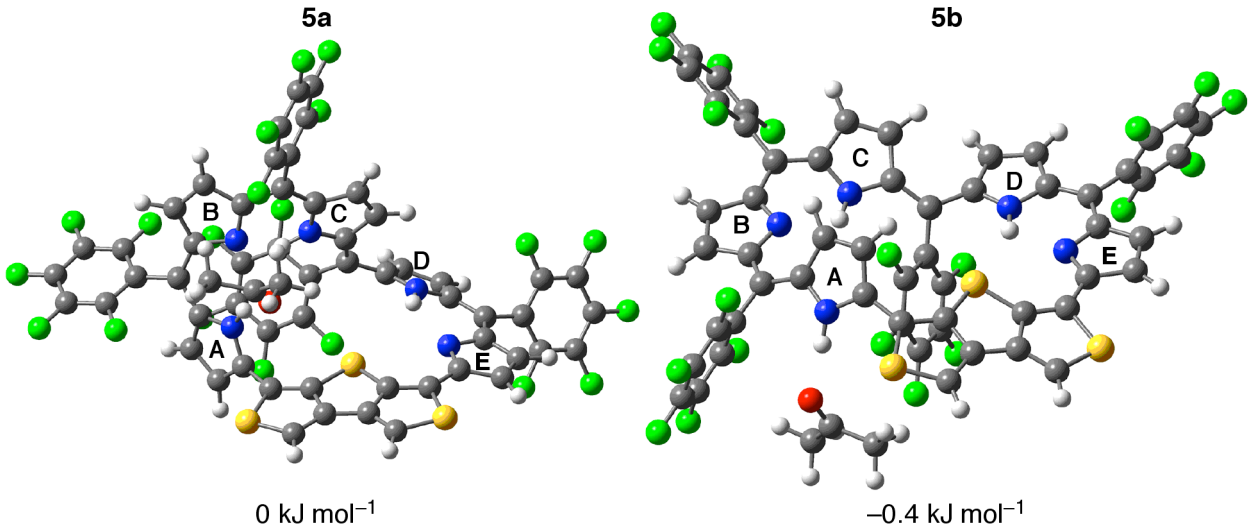

Figure S16. The optimized structures and relative energies of [28]hexaphyrin **5a** and **5b** with one acetone molecule.

Table S4. The relative total energies (kJ mol^{-1}) of **5a** and **5b** with one solvent molecule.

	5a+DMF	**5b**+DMF	**5a**+acetone	**5b**+acetone
B3LYP/6-311G(d,p)	0	–6.2	0	–0.4
CAM-B3LYP/6-311G(d,p)	0	–5.6	0	–1.4
M06-2X/6-311G(d,p)	0	–3.1	0	–0.5

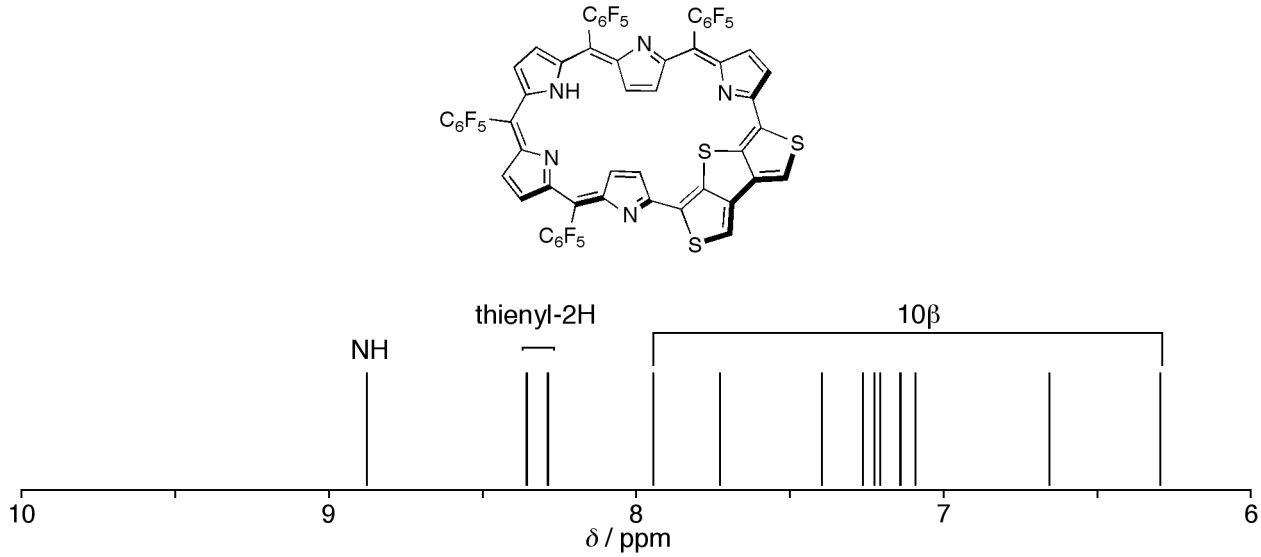

Figure S17. Simulated ^{1}H chemical shifts and the NICS value at the gravity center on the optimized structure of **6**.

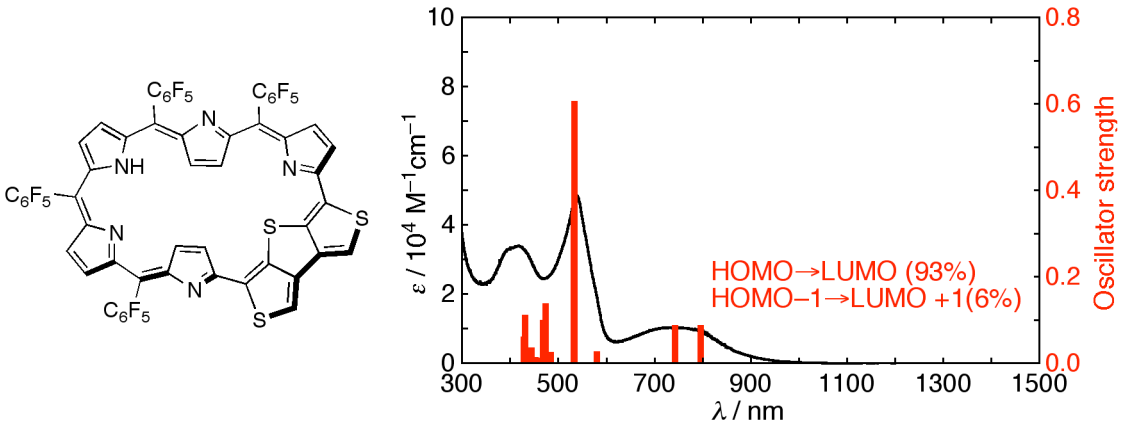

Figure S18. The UV/vis/NIR absorption spectra of **6** in CH_2Cl_2 (black) and calculated excitation energies with oscillator strengths on the optimized structure of **6** (red). The excitation weights of the lowest excitation are indicated.

Table S5. The calculated bond lengths (Å) and NBO bond orders on the β-DTT units.

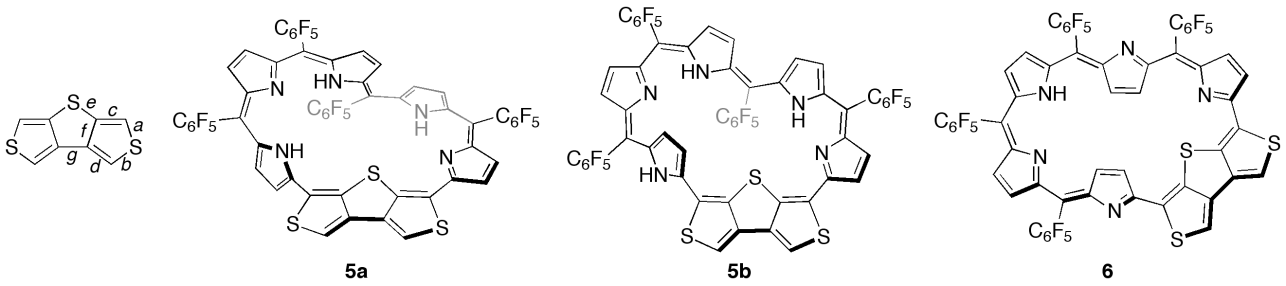

	Bond length (Å)			NBO bond order		
Bond	**5a**	**5b**	**6**	**5a**	**5b**	**6**
a	1.765	1.768	1.759	1.1289	1.1278	1.1306
	1.768	1.764	1.756	1.1243	1.1276	1.1366
b	1.728	1.726	1.739	1.2346	1.2369	1.2324
	1.725	1.733	1.736	1.2353	1.2238	1.2449
c	1.382	1.379	1.378	1.4453	1.4609	1.4187
	1.375	1.374	1.377	1.5275	1.4975	1.4505
d	1.372	1.371	2.374	1.5056	1.5082	1.5084
	1.369	1.371	1.374	1.5267	1.5228	1.5077
e	1.774	1.774	1.748	1.0904	1.0791	1.1137
	1.787	1.784	1.767	1.0649	1.0644	1.1032
f	1.436	1.439	1.434	1.1958	1.1930	1.1944
	1.443	1.438	1.436	1.1771	1.1833	1.1927
g	1.450	1.451	1.460	1.0683	1.0674	1.0652

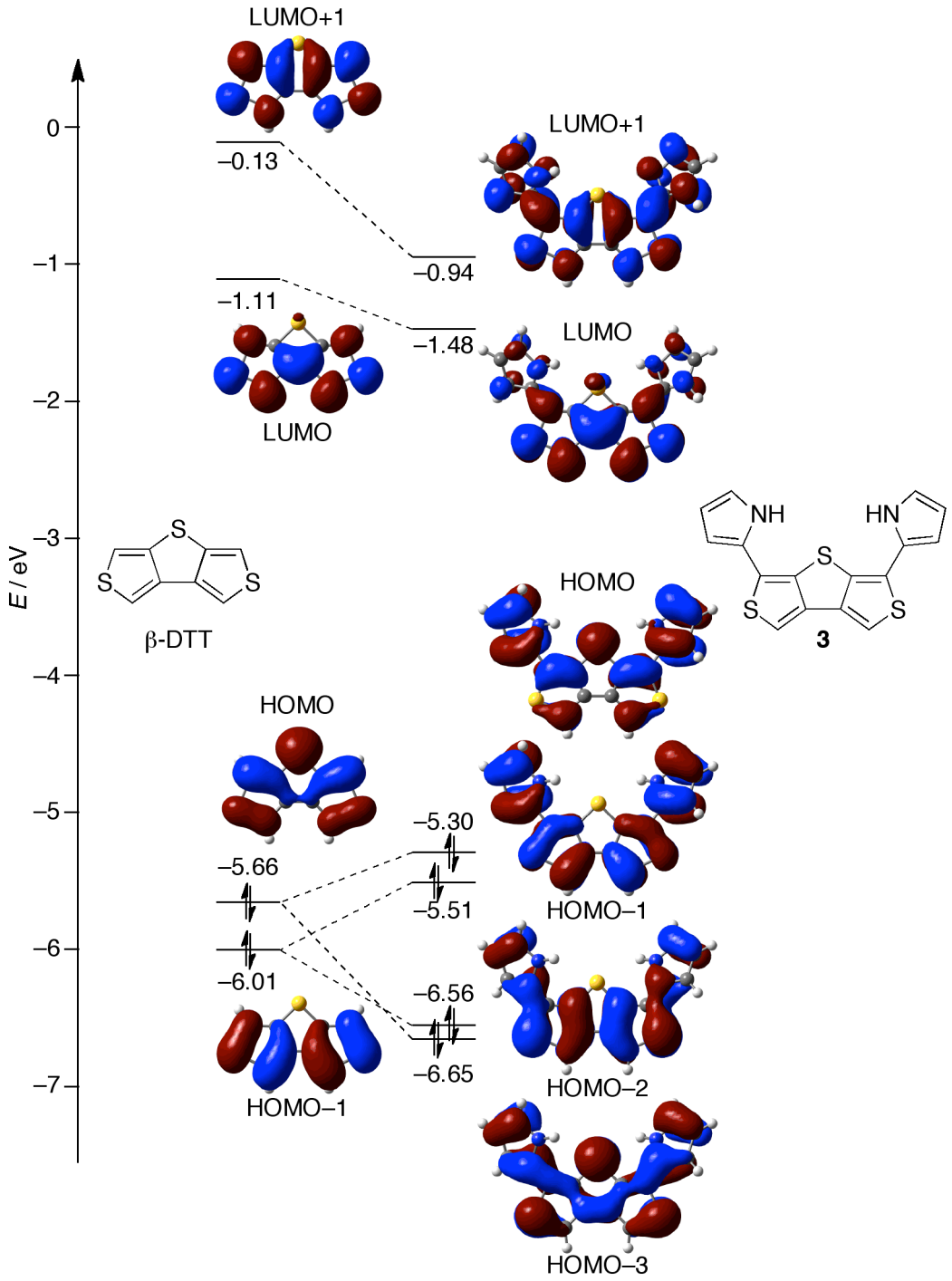

Figure S19. Selected Kohn-Sham orbitals of β-DTT and **3**.

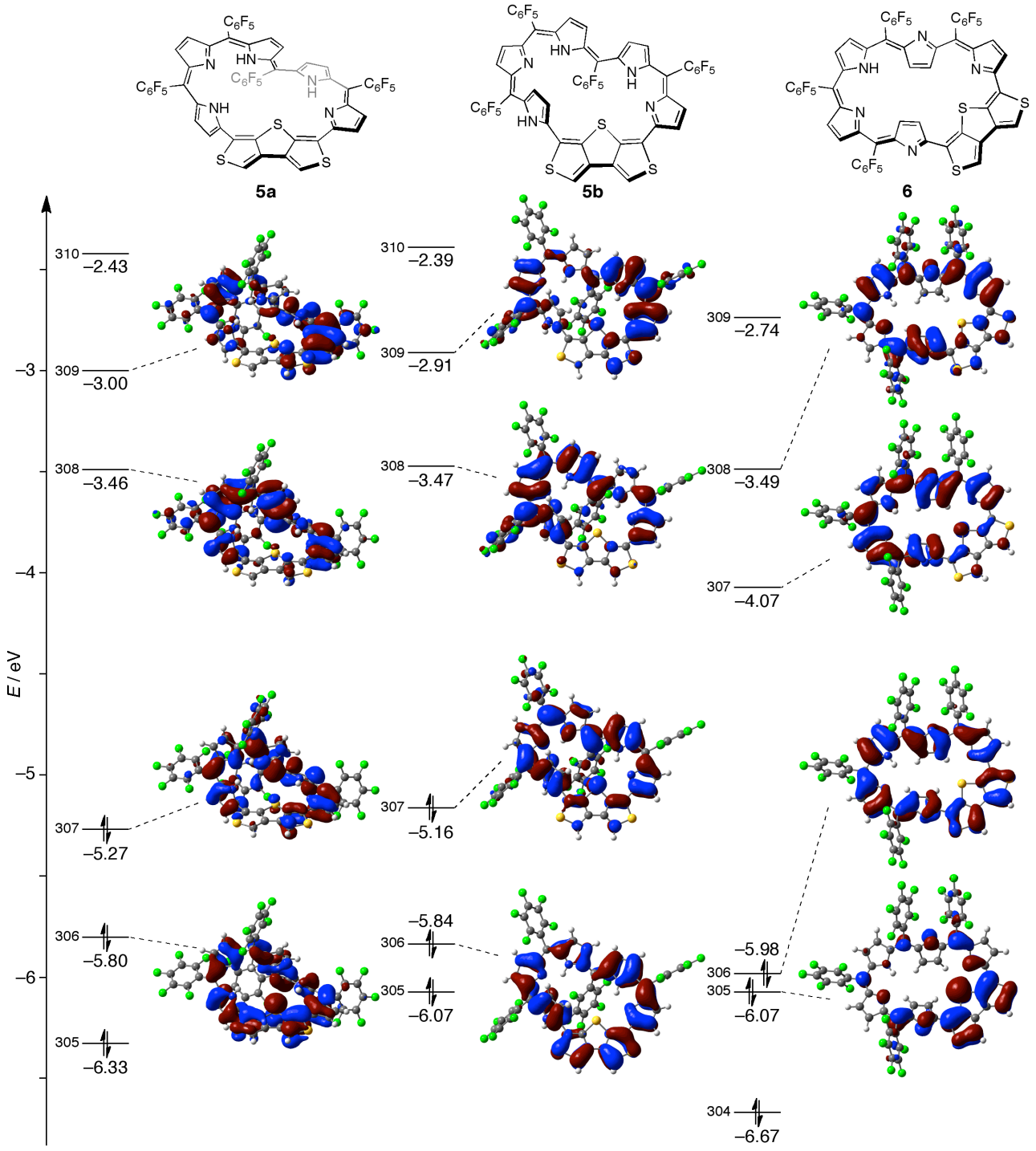

Figure S20. Selected Kohn-Sham orbitals of hexaphyrins **5a**, **5b**, and **6**.

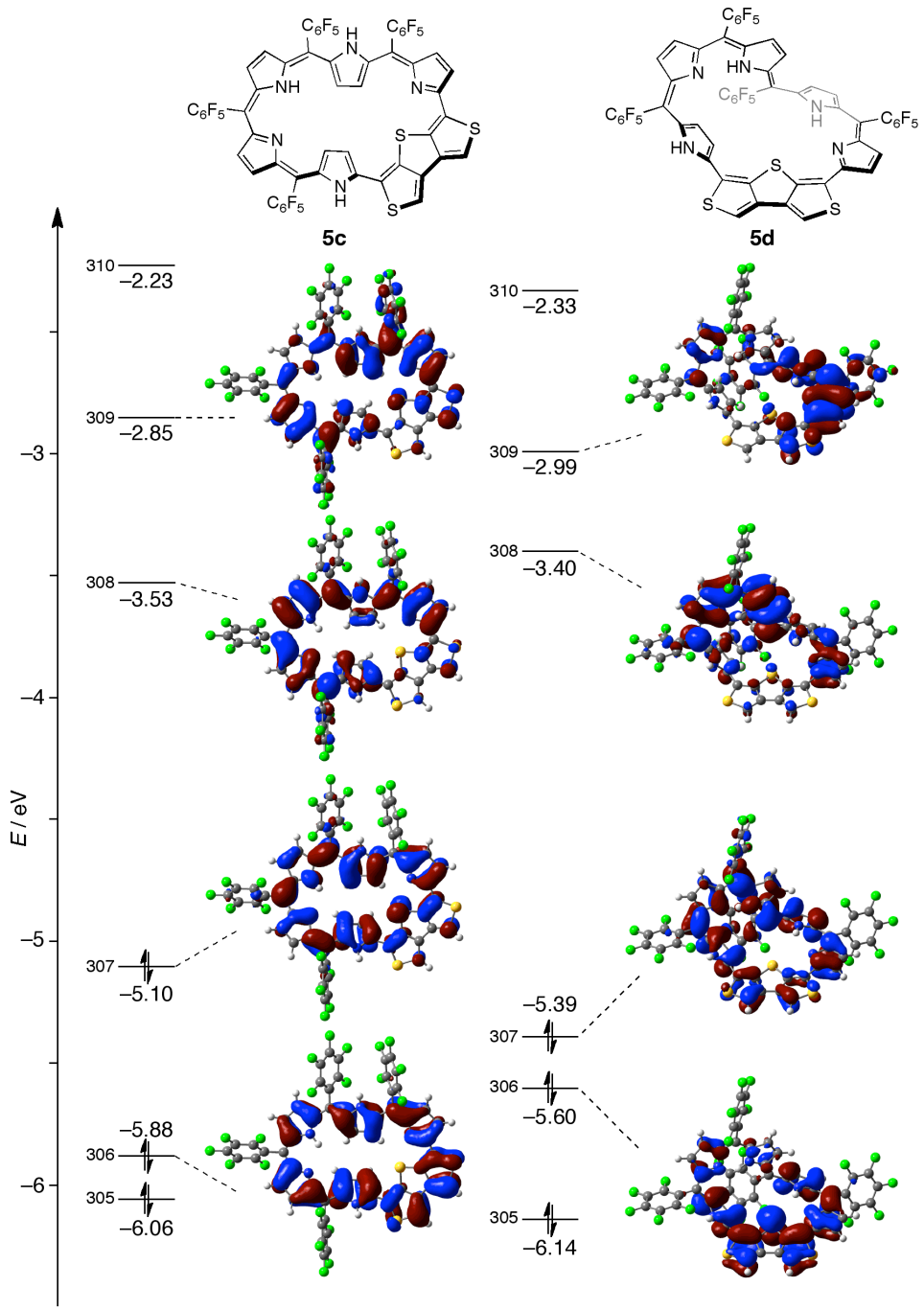

Figure S21. Selected Kohn-Sham orbitals of hexaphyrins **5c** and **5d**. Similar to **5b**, the HOMO of **5c** indicates the involvement of p_z orbital of the central sulfur atom. On the other hand, similar to **5a** and **6**, the HOMO of **5d** has no contribution of p_z orbital. Thus, the cyclic 28π-system and linear π-system should be dominant for **5c** and **5d**, respectively, as simulated by the NMR and TD-DFT calculations (Figures S12 and S15).

9. References

[S1] M. J. Frisch, G. W. Trucks, H. B. Schlegel, G. E. Scuseria, M. A. Robb, J. R. Cheeseman, G. Scalmani, V. Barone, B. Mennucci, G. A. Petersson, H. Nakatsuji, M. Caricato, X. Li, H. P. Hratchian, A. F. Izmaylov, J. Bloino, G. Zheng, J. L. Sonnenberg, M. Hada, M. Ehara, K. Toyota, R. Fukuda, J. Hasegawa, M. Ishida, T. Nakajima, Y. Honda, O. Kitao, H. Nakai, T. Vreven, J. A. Montgomery, Jr., J. E. Peralta, F. Ogliaro, M. Bearpark, J. J. Heyd, E. Brothers, K. N. Kudin, V. N. Staroverov, T. Keith, R. Kobayashi, J. Normand, K. Raghavachari, A. Rendell, J. C. Burant, S. S. Iyengar, J. Tomasi, M. Cossi, N. Rega, J. M. Millam, M. Klene, J. E. Knox, J. B. Cross, V. Bakken, C. Adamo, J. Jaramillo, R. Gomperts, R. E. Stratmann, O. Yazyev, A. J. Austin, R. Cammi, C. Pomelli, J. W. Ochterski, R. L. Martin, K. Morokuma, V. G. Zakrzewski, G. A. Voth, P. Salvador, J. J. Dannenberg, S. Dapprich, A. D. Daniels, O. Farkas, J. B. Foresman, J. V. Ortiz, J. Cioslowski, and D. J. Fox, Gaussian *Gaussian 09*, revision D.01; Gaussian, Inc.; Wallingford, CT, 2013.

[S2] A. D. Becke, *J. Chem. Phys.* 1993, **98**, 1372.

[S3] C. Lee, W. Yang and R. G. Parr, *Phys. Rev. B: Condens. Matter Mater. Phys.*, 1988, **37**, 785.

[S4] T. Higashino, A. Kumagai and H. Imahori, *Chem. Commun.*, 2017, **53**, 5091.

[S5] V. G. Anand, S. Saito, S. Shimizu and A. Osuka, *Angew. Chem., Int. Ed.*, 2005, **44**, 7244.

[S6] G. M. A. Junqueira and H. F. Dos. Santos, *J. Mol. Model.*, 2014, **20**, 2152.

[S7] Y. Valadbeigi, *Comput. Theor. Chem.*, 2017, **1102**, 44.